Check for updates

Small

NANO · MICRO small
www.small-journal.com

RESEARCH ARTICLE

Multifunctional Triboelectric Textiles With Synergistically Photoinduced Enhanced Output Performance, Reprocessability, and Closed-Loop Recyclability

Ruirui Cao[1,2] | Xin Li[1] | Jiaxin Yu[1] | Yuqing Zhou[1] | Le Li[1] | Wenbo Dong[1] | Fumin Li[1] | Huilin Li[1] | Ying Liu[1] | Caofeng Pan[2]

[1]Henan Key Laboratory of Quantum Materials and Quantum Energy, School of Future Technology, Henan University, Kaifeng, China | [2]Institute of Atomic Manufacturing, International Research Institute For Multidisciplinary Science, Beihang University, Beijing, China

Correspondence: Ruirui Cao (rrcao0403@vip.henu.edu.cn) | Fumin Li (lifm@henu.edu.cn) | Caofeng Pan (pancaofeng@buaa.edu.cn)

Received: 8 June 2026 | **Revised:** 7 July 2026 | **Accepted:** 24 August 2026

Keywords: closed-loop recyclability | multifunctional integration | photoinduced enhance | triboelectric textiles

ABSTRACT

The development of conventional polymer-based triboelectric materials (PTMs) faces two critical bottlenecks: the irreconcilable conflict between durability and recyclability, and the inherently limited interfacial charge generation and retention that constrain output performance. This study adopted a free radical copolymerization-thermally reversible Diels-Alder (DA) cascade reaction strategy, combined with viscosity regulation and in situ crosslinked electrospinning technology, to successfully fabricate a dynamically covalent crosslinked network-based PTM with $CsPbBr_3$@KBr perovskite functional filler, resulting in multifunctional and synergistically optimized textile-based TENGs (DCCNF-based TENGs). Experimental results demonstrate that DCCNFs exhibit enhanced output performance, self-healing capability, photoluminescent and photoinduced-enhanced functions, and closed-loop recyclability. Compared with undoped DCCNF0, the DCCNF4-based TENG increased to approximately 2.25-fold, 5.78-fold, 3.13-fold, and 3.46-fold enhancements in terms of V_{oc}, I_{sc}, Q_{sc}, and power density, respectively. Under UV and sunlight irradiation, the photoelectric-triboelectric coupling synergistic effect further significantly enhances the current density of the series DCCNF-based TENGs. Importantly, the output improvement is due to filler-induced dielectric modulation, enhanced surface charge trapping, and the photoelectric effect. Collectively, these DCCNF-based TENGs effectively address the dual bottlenecks of output performance and sustainability of triboelectric technology, while offering a versatile platform for next-generation sustainable smart wearable systems.

1 | Introduction

The booming development of the Internet of Things (IoT) has given rise to a vast number of independent sensor nodes, creating a massive demand for portable and distributed power sources [1–3]. Consequently, the power supply issue has increasingly become a critical bottleneck constraining its further advancement [4–6]. Triboelectric nanogenerators (TENGs), capable of efficiently harvesting and converting minute mechanical energy from the ambient environment into electricity, boast advantages such as low cost, facile fabrication, and high energy conversion efficiency [7–9]. They are progressively emerging as one of the pivotal technologies to address the distributed power supply challenges for wireless sensor networks [10, 11]. Within TENG application frameworks, where they serve as either the core power supply units or functional components for human-machine interaction interfaces and self-powered sensing systems, their cyclic stability and high output performance are paramount

All rights reserved, including rights for text and data mining and training of artificial intelligence technologies or similar technologies.
© 2026 Wiley-VCH GmbH

[12]. The output performance of TENGs core depends fundamentally on its triboelectric interface charge density, which is jointly governed by the charge retention capability (i.e., charge trap density) of the paired triboelectric materials and their contact work function difference [13–15].

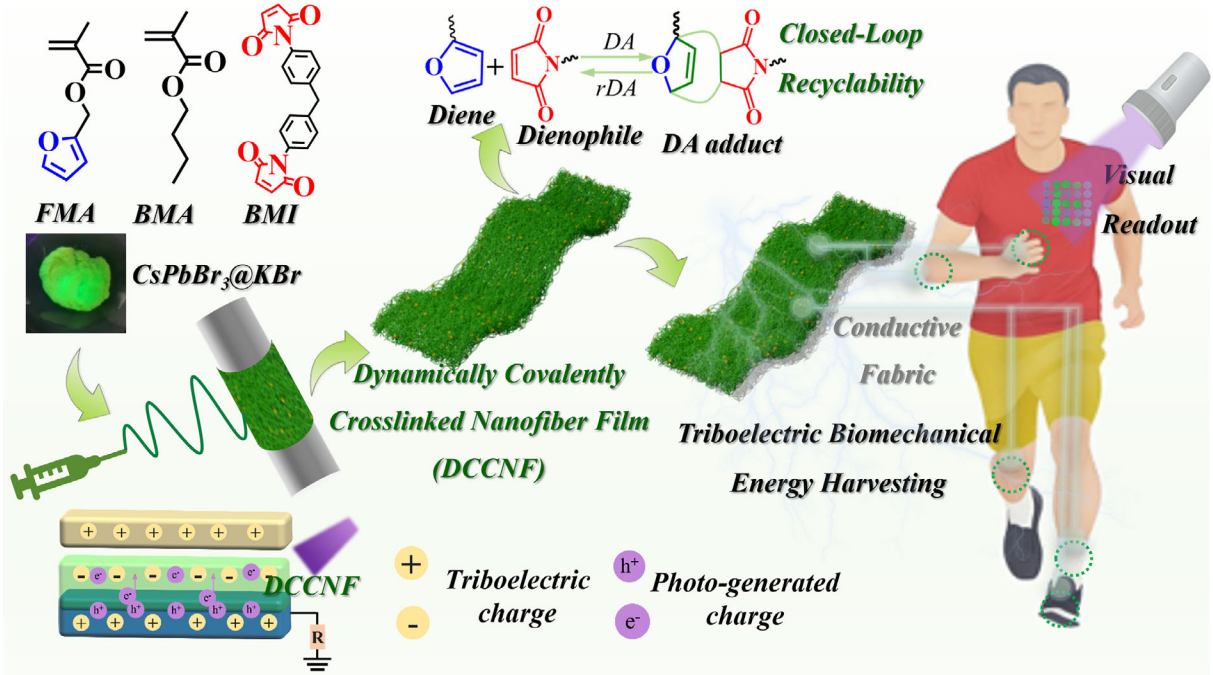
Polymer-based triboelectric materials (PTMs), owing to their exceptional flexibility, mechanical strength, processability, and tunable dielectric properties, have established as the cornerstone of TENG technology [16]. Particularly, polymer nanofibres exhibit significant advantages for diverse distributed energy management scenarios, owing to their in situ polarization potential, high specific surface area, tunable surface roughness, and excellent functional integration compatibility [17–19]. However, the advancement of conventional PTMs remains constrained by two fundamental bottlenecks [20, 21]. First, the inherent conflict between durability and recyclability proves challenging to reconcile, severely impeding the development and application of novel high-performance PTMs [22]. Specifically, thermoplastic polymers offer favorable processability but frequently exhibit inadequate mechanical strength and thermal stability, limiting the application potential of their nanofibers [23]. Conversely, thermoset polymers exhibit superior durability, but their highly crosslinked three-dimensional network structures make depolymerization and recycling extremely difficult, leading to resource waste and a substantial environmental footprint [20, 21]. Second, the low output performance of PTMs, particularly their current density, restricts further application expansion [13–15, 24]. Although the inherently high bulk resistivity of PTMs has been considered a limiting factor, we demonstrate that the output can be substantially enhanced without modifying bulk conductivity. Consequently, there is an urgent imperative to design and develop novel PTMs that simultaneously deliver high output performance (especially high current density), exceptional cyclic durability, and closed-loop recyclability, coupled with efficient nanofiber fabrication. This integration is paramount for constructing next-generation high-performance, multifunctional TENG devices and underpinning the sustainable development of IoT.

Recently, covalently adaptable networks have emerged as a novel class of dynamically crosslinked polymers that integrate the structural stability of thermoset materials with the reconfigurability of thermoplastic materials, offering an innovative paradigm for designing high-performance and sustainable polymer materials, which hold promise for advancing the next generation of high-performance nanofibers [25, 26]. Recent research by Li et al. provides compelling evidence for this strategy [22, 27]. Utilizing a thermally reversible Diels-Alder (DA) dynamic covalent crosslinking strategy, integrated with viscosity regulation and in situ cross-linked electrospinning technology, they successfully fabricated dynamically covalent cross-linked polymer nanofibers possessing closed-loop recyclability, exceptional flexibility, and robust thermal stability. This material system innovatively merges the high stability inherent in thermoset polymers with the processability of thermoplastics, enabling it to maintain structural integrity under service conditions while enabling reversible topological network reconstruction or polymer chain depolymerization upon specific external stimuli, such as thermal activation [28, 29]. This advancement provides not only an effective solution to the core challenge of balancing durability and recyclability in polymer materials but also lays a robust material foundation for developing high-performance polymer nanofiber-based PTMs that possess both superior durability and closed-loop recycling potential.

Concurrently, the incorporation of functional fillers into PTMs represents a proven strategy for continuously enhancing TENG output performance [30, 31], which not only improves electrical output by optimizing dielectric properties or enhancing charge-trapping effects but also preserves the mechanical flexibility of the composite PTMs [7–9, 32]. Among various candidate fillers, halide perovskite materials have garnered significant attention due to their unique physicochemical properties [33]. Their tunable band structure, efficient charge-trapping capability, superior dielectric characteristics, and pronounced ferroelectric polarization effect render them ideal additives for augmenting both the charge-trapping capacity and interfacial electrostatic potential of PTMs [13–15, 34]. Furthermore, halide perovskites exhibit exceptional optoelectronic properties, low resistivity, and high carrier mobility, positioning them as promising multifunctional photoelectric-triboelectric materials with substantial development potential in hybrid TENGs [35, 36]. In 2020, Tang et al. first elucidated the physical mechanism underlying the synergistic enhancement of triboelectric charge density by photogenerated carriers [37]. Integrating photoactive components (e.g., perovskites) into TENGs enables the dynamic modulation of tribo-interface charge density via photogenerated carriers (i.e., synergistic coupling of photovoltaic and triboelectric effects at the interface), thereby significantly boosting the current output levels of TENGs under light exposure [24, 38, 39]. Importantly, this improvement does not rely on reducing the bulk resistivity of the polymer matrix, but rather on filler-induced dielectric modulation, enhanced surface charge trapping, and the photoelectric effect. This mechanism effectively overcomes the bottleneck limiting output current in conventional TENGs, highlighting the profound value of photovoltaic-triboelectric composite technology [24, 40, 41]. In summary, integrating dynamically covalent cross-linked polymer possessing closed-loop recyclability with optoelectronic functional halide perovskite fillers to develop novel hybrid TENGs based on halide perovskite-doped PTMs represents an effective new pathway, which enables the synchronous and efficient harvesting of both mechanical energy and light energy (the most abundant renewable energy source besides mechanical energy), thereby overcoming the dual bottlenecks of output performance and sustainability in TENG technology.

However, most current photoinduced enhanced TENGs utilize organic-inorganic hybrid perovskites as the photoactive material [36, 42]. While these materials exhibit exceptional optoelectronic properties and tunable bandgaps owing to their unique crystal structure and compositional tunability, making them highly suitable for optoelectronic devices such as solar cells, light-emitting diodes, and photodetectors, their inherent instability under environmental factors (e.g., humidity, heat, and light) leads to rapid performance degradation of the relevant devices [36, 43, 44]. This instability constitutes a fundamental challenge impeding the practical deployment of various perovskite-based devices, including hybrid TENGs. Therefore, there is an urgent need to develop perovskite materials with high environmental stability to enhance the long-term operational stability of perovskite-based hybrid TENGs under complex operating conditions.

16136829, 0, Downloaded from https://onlinelibrary.wiley.com/doi/10.1002/smll.75667 by Beihang University (Buaa), Wiley Online Library on [23/09/2026]. See the Terms and Conditions (https://onlinelibrary.wiley.com/terms-and-conditions) on Wiley Online Library for rules of use; OA articles are governed by the applicable Creative Commons License



SCHEME 1 | Schematic diagram of the fabrication process, structural architecture, operational mechanism, and multifunctional integration of DCCNF-based TENG devices.

To address the above challenges, as shown in Scheme 1, this study proposes a novel design strategy for multifunctional photoelectric-triboelectric PTMs, which can synergistically optimize environmental tolerance, energy conversion efficiency, and recyclability. Specifically, a dynamic covalent cross-linked polymer network (DA adduct) was employed as the PTM matrix, ingeniously reconciling the contradiction between the durability and recyclability of conventional polymers. Meanwhile, $CsPbBr_3$@KBr all-inorganic photoluminescent perovskite was selected as the functional filler. The KBr salt shell creates a Br-rich environment to passivate surface defects and, together with the PTM, acted as a protective matrix to enhance the environmental stability of the perovskite material, achieving functional coupling and synergistic optimization of the triboelectric and photoelectric effects. Ultimately, by utilizing viscosity regulation and in situ electrospinning technology, $CsPbBr_3$@KBr-doped PTMs were successfully developed, exhibiting self-healing capability, photoluminescent and photoinduced enhanced functions, and closed-loop recyclability. Based on this, a series of high-performance TENGs possessing efficient and stable operation, high energy conversion efficiency, and sustainable characteristics were constructed. This strategy is anticipated to provide new insights and methodologies for the further development of TENG technology and promote its widespread adoption in fields such as IoT.

2 | Results and Discussion

2.1 | Design Concept and Construction of Multifunctional Triboelectric Textiles

As previously discussed, TENGs, serving as core components in human-machine interfaces and self-powered sensing systems, necessitate the efficient integration of multifunctional properties, particularly cycling stability and high output performance, to enhance their comprehensive performance and drive application expansion [12, 45]. As illustrated in Scheme 1, this study employed furfuryl methacrylate (FMA), butyl methacrylate (BMA), and bismaleimide (BMI) as raw materials. The FMA-*co*-BMA copolymer was synthesized via free radical copolymerization. Then, utilizing this copolymer as the diene and BMI as the dienophile [46, 47], a dynamically covalent cross-linked polymer network with reprocessability and closed-loop recyclability was constructed through a thermally reversible DA reaction [22]. On this basis, highly stable $CsPbBr_3$@KBr photoluminescent perovskite fillers were prepared using a direct water evaporation crystallization method [48]. Subsequently, a series of multifunctional triboelectric textiles (dynamic covalently crosslinked nanofibers, DCCNFs) were fabricated through electrospinning, simultaneously achieving photo-induced output enhancement, reprocessability, and closed-loop recyclability. This textile enables efficient mechanical energy harvesting alongside visual information retrieval under dark-field conditions.

2.2 | Composition, Physicochemical, and Morphological Characteristics of DCCNFs

As illustrated in Figure 1a, a dynamically covalent cross-linked polymer (i.e., DA adduct), synthesized via a thermally reversible DA reaction, was employed as the triboelectric matrix. Utilizing $CsPbBr_3$@KBr all-inorganic perovskite as the functional filler, the DCCNFs were prepared through viscosity regulation and in situ cross-linked electrospinning technology. The dynamically covalent cross-linked polymer was constructed via [4+2] cycloaddition between furan groups and maleimide groups [49, 50], using the FMA-*co*-BMA copolymer (structural characterization

16136829, 0, Downloaded from https://onlinelibrary.wiley.com/doi/10.1002/smll.75667 by Beihang University (Buaa), Wiley Online Library on [23/09/2026]. See the Terms and Conditions (https://onlinelibrary.wiley.com/terms-and-conditions) on Wiley Online Library for rules of use; OA articles are governed by the applicable Creative Commons License

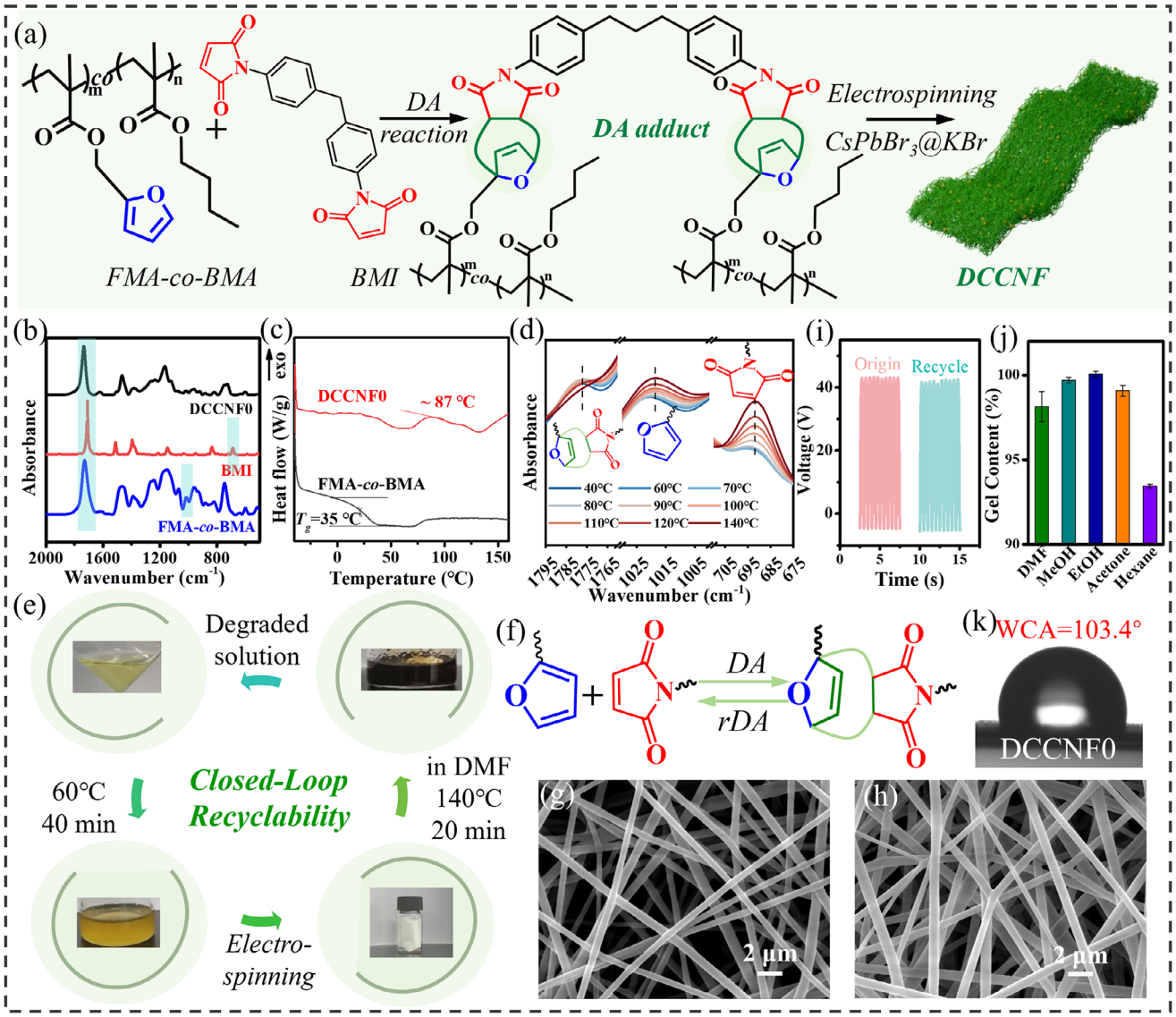


FIGURE 1 | (a) Fabrication process of DCCNFs via Diels-Alder (DA) reaction and electrospinning technology. (b) ATR-FTIR spectra of DA adduct (DCCNF0), BMI, and FMA-*co*-BMA. (c) DSC curves of DCCNF0 and FMA-*co*-BMA. (d) ATR-FTIR spectra of DCCNF0 under varying temperatures. (e) Schematic diagram and (f) mechanism illustration of the closed-loop recyclability of DCCNFs. SEM images of (g) original and (h) recycled DCCNF0. (i) V_{oc} of the original and recycled DCCNF0-based TENG. (j) Gel content of DCCNF0 under different solvents at room temperature. (k) Water contact angle (WCA) of DCCNF0.

in Figure S1a–c), prepared through free radical copolymerization, as the diene and BMI as the dienophile. The FTIR spectra in Figure 1b reveal that the intensity of the characteristic peaks at 1018 cm^{-1} (attributed to the asymmetric C-O-C stretching vibration of the furan ring in FMA-*co*-BMA) and 685 cm^{-1} (attributed to the imide ring vibration in BMI) in the DCCNFs significantly attenuates to the point of disappearance, confirming the complete reaction between FMA-*co*-BMA and BMI. Concurrently, a new vibration peak emerges at 1777 cm^{-1}, attributed to C-O/C-N bonds in the six-membered ring of the DA adduct. Additionally, the C = O peak of the imide ring in BMI undergoes a blue shift due to cyclic reconstruction [51–53]. These results fully validate the occurrence of an efficient cyclization cross-linking reaction and the successful construction of the cross-linked network within the DCCNF film.

As illustrated in the DSC curves shown in Figure 1c, the glass transition temperature (T_g) of FMA-*co*-BMA is approximately 35°C. After DA reaction crosslinking, the T_g of DCCNFs increases significantly, attributable to the polymer structural reconstruction [54, 55]. Further analysis reveals a prominent endothermic peak around 87°C, corresponding to the thermally induced retro-DA (rDA) dissociation process of the DA adduct (Figure 1f). From the variable-temperature FTIR spectra of the DCCNF0 in Figure 1d, it can be observed that, below 90°C, the C = O stretching vibration characteristic peak at 1777 cm^{-1} in DA adducts remains stable, confirming the structural integrity of DCCNFs and indicating their stable existence. As the temperature rises, characteristic peaks at 1018 cm^{-1} (furan groups in diene FMA-*co*-BMA) and 692 cm^{-1} (maleimide groups in dienophile BMI) emerge and intensify progressively, while the intensity of the peak at 1777 cm^{-1} attenuates synchronously. This inverse

16136829, 0, Downloaded from https://onlinelibrary.wiley.com/doi/10.1002/smll.75667 by Beihang University (Buaa), Wiley Online Library on [23/09/2026]. See the Terms and Conditions (https://onlinelibrary.wiley.com/terms-and-conditions) on Wiley Online Library for rules of use; OA articles are governed by the applicable Creative Commons License

correlation provides compelling evidence for the thermo-reversible response of DCCNFs [54, 55]. As shown in Figure 1e, leveraging the thermal reversibility of DA dynamic cross-linking (Figure 1f), the prepared DCCNFs exhibit excellent closed-loop recyclability. The preparation process involves dissolving FMA-*co*-BMA and BMI at a certain ratio in DMF, reacting at 60°C for 40 min, and then directly electrospinning the reaction solution to obtain DCCNFs (Figure 1g). For recycling, DCCNFs are dissolved in DMF (28 wt.%, matching the spinning solution) and treated at 140°C for 20 min to trigger the rDA degradation. For reprocessing, despite solution discoloration from side reactions (e.g., double bond oxidation) [22], the degraded solution can be successfully regenerated into nanofibers through in situ cross-linking electrospinning after heating and adjusting the viscosity to approximately 80 cps (Figure 1h). SEM analysis (Figure 1g,h and Figure S3e) shows that the regenerated DCCNF0 maintains pristine morphology, with uniformly distributed fiber diameters that only slightly increase, and its triboelectric output performance remains unattenuated (Figure 1i). This fully confirms its excellent reprocessability and closed-loop recyclability, thereby endowing PTMs with good sustainability. Furthermore, as shown in Figure 1j,k and Figure S4, DCCNFs exhibit good hydrophobicity and superior solvent resistance. After 24 h immersion in various organic solvents, the gel retention rate still exceeds 90%, confirming exceptional anti-swelling capacity and structural stability. Combined with SEM characterization (Figure S4), it can be concluded that the covalently cross-linked network of DCCNFs has strong stability in complex chemical environments, making them suitable for long-term service scenarios.

As previously outlined, the development of conventional PTMs faces two critical bottlenecks. Firstly, the irreconcilable conflict between durability and recyclability severely restricts the research, development, and application of novel high-performance nanofiber-based PTMs [22]. In this study, dynamically covalent crosslinked networks based DCCNFs were fabricated, which ingeniously reconcile the high stability of thermosetting polymers with the easy processability of thermoplastics. These DCCNFs can maintain structural integrity during service while enabling polymer chain depolymerization under thermal stimuli, effectively resolving the durability-recyclability paradox in conventional PTMs. Secondly, the intrinsically limited interfacial charge generation and retention of PTMs constrain their output performance, particularly current density [13–15, 24]. To address this, we adopted a direct aqueous evaporation crystallization method (adapted from prior methodologies) to synthesize salt-shell metal halide perovskite ($CsPbBr_3$@KBr, Figure S1d–h) [48]. The KBr salt-shell simultaneously provides a Br-rich environment for surface defect passivation and, together with DA adduct, acts as a protective matrix to shield the active core from environmental degradation, significantly enhancing material stability.

Building upon the above foundations, a series of $CsPbBr_3$@KBr-doped DA adduct-based DCCNFs were fabricated via in situ crosslinking electrospinning, which served as triboelectric functional layers to construct single-electrode mode TENGs (structural configuration in Figure 2a, working mechanism in Figure S5a). SEM characterization (Figure S2) reveals that all DCCNF samples exhibited smooth-surfaced nanofiber morphology with uniform diameter distribution. Notably, the nanofiber diameter demonstrated a gradient increase with rising $CsPbBr_3$@KBr doping content (Figure S2e). Further observation, as depicted in Figure 2b and Figures S3a,b, indicated that $CsPbBr_3$@KBr was uniformly encapsulated within the nanofibers. This structural feature could significantly enhance the material's long-term service stability [56]. Additionally, thermogravimetric analysis (Figure S3c) indicated that the thermal decomposition temperature of DCCNFs reached 250°C, showcasing excellent thermal stability. Concurrently, the $CsPbBr_3$@KBr incorporation significantly elevated the water contact angle from 103.4° (DCCNF0) to 121.7° (DCCNF4), endowing the DCCNFs with enhanced hydrophobicity (Figure S3d). This property confers integrated waterproofing, anti-fouling, and self-cleaning capabilities to DCCNFs. Critically, the resultant hydrophobic barrier effectively mitigates moisture ingress into the perovskite phase [57, 58], thereby further enhancing the environmental stability of the halide perovskite components.

2.3 | Triboelectric Characteristics of DCCNF Based TENGs

As shown in Figure 2c–e, the influence of the doping amount of $CsPbBr_3$@KBr on the triboelectric output performance of DCCNFs was systematically investigated. Relevant results revealed that with the increase in the doping amount, the electrical output of the corresponding TENG device exhibited a trend of first increasing and then decreasing, reaching a peak at a doping amount of 4 wt.%. Compared with undoped DCCNF0, the DCCNF4-based TENG exhibited approximately 2.25-fold, 5.78-fold, and 3.13-fold enhancements in V_{oc}, I_{sc}, and Q_{sc}, respectively. Furthermore, the power density increased from the initial 964 μW/m^2 (DCCNF0) to 3333 μW/m^2 (DCCNF4), representing an increase of 246% (Figure 2f). Subsequently, the electrostatic potential field distribution within the TENG device was simulated using COMSOL Multiphysics. Simulation results demonstrate a significantly enhanced potential intensity distribution at the DCCNF4/Al film interface compared to the undoped DCCNF0/Al film counterpart (Figure S5b). It is well-known that the intrinsic properties of PTMs fundamentally determine the output performance of TENGs, where dielectric constant and surface potential are positively correlated with the output performance [59, 60]. Studies have shown that improving the electrical output performance of the PTMs requires synergistic optimization—enhancing the dielectric constant to boost charge storage capacity and suppressing dielectric loss to reduce energy dissipation [61–63]. However, an increase in the dielectric constant is often accompanied by an increase in dielectric loss, which limits further performance improvement and may even reduce the electrical output.

To this end, this study systematically characterized the dielectric properties (dielectric constant and dielectric loss) and surface potential of the series DCCNFs (Figure 2g--i). The results indicated that the dielectric constant and surface potential of all doped DCCNFs increased monotonically with the doping amount of $CsPbBr_3$@KBr (Figure 2g,i), which slightly differed from the triboelectric test results. In contrast, the dielectric loss was

16136829, 0, Downloaded from https://onlinelibrary.wiley.com/doi/10.1002/smll.75667 by Beihang University (Buaa), Wiley Online Library on [23/09/2026]. See the Terms and Conditions (https://onlinelibrary.wiley.com/terms-and-conditions) on Wiley Online Library for rules of use; OA articles are governed by the applicable Creative Commons License

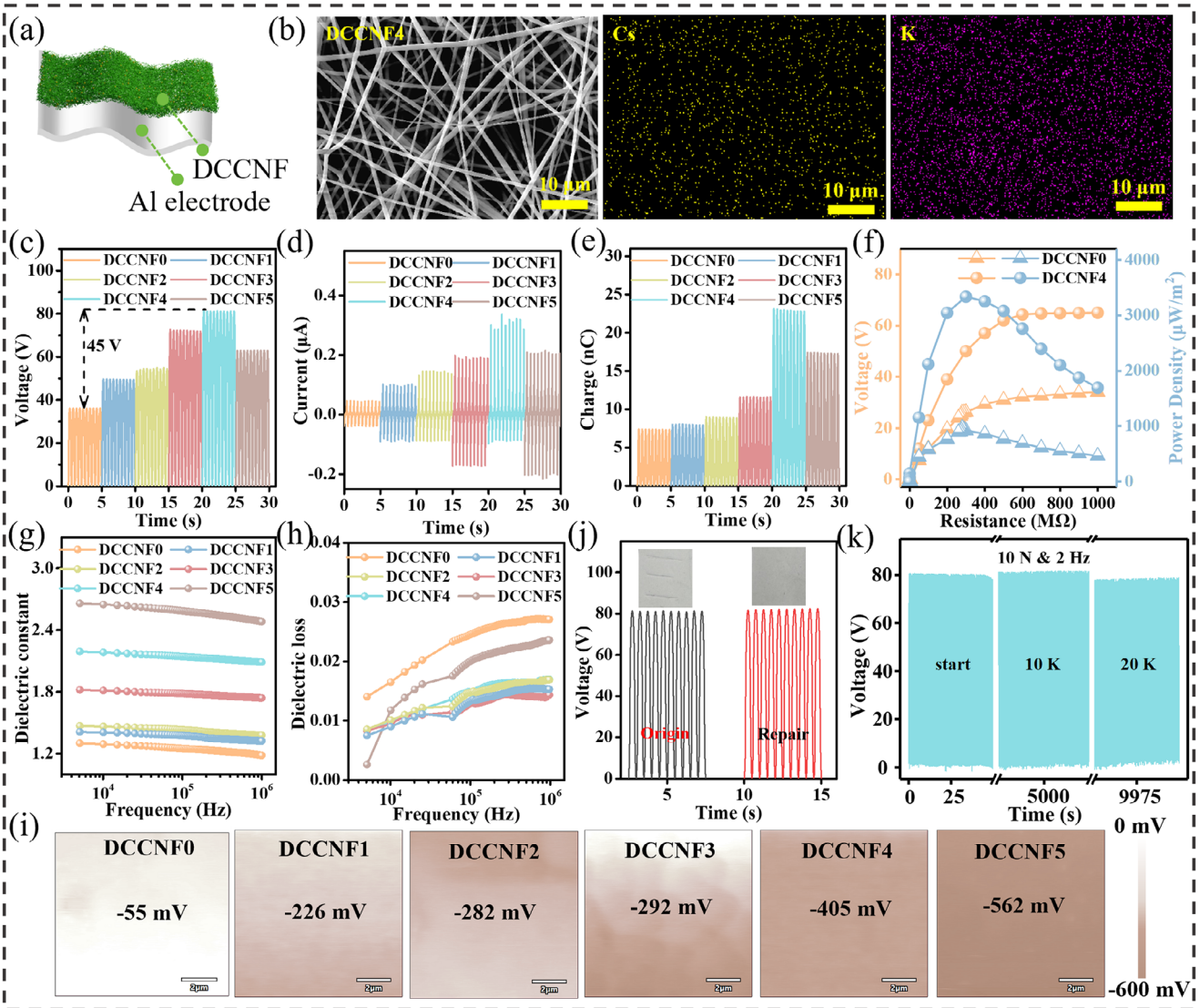


FIGURE 2 | (a) Schematic diagram of DCCNF-based TENG. (b) SEM image and elemental mapping images of DCCNF4. (c–e) Electrical outputs of the series DCCNFs. (f) Power density output of DCCNF0 and DCCNF4 at different load resistors. (g) Dielectric constant, (h) dielectric loss, and (i) KPFM images of the series DCCNFs. (j) V_{oc} of the original and repaired DCCNF4. (k) Stability test of DCCNF4 for more than 20,000 cycles.

significantly lower than that of DCCNF0 when the doping amount was ≤4 wt.% (Figure 2h). This trend contrasted with the non-monotonic change in triboelectric output. Mechanistic studies revealed that while elevated dielectric constant enhances charge storage, increased dielectric loss exacerbates interfacial charge dissipation [61–63]. At 5 wt.% doping (DCCNF5), the dielectric loss increased abnormally (Figure 2h), leading to a decrease in energy storage efficiency. Consequently, a 4 wt.% doping of $CsPbBr_3$@KBr in this study achieved a synergistic optimization of maximizing the dielectric constant and minimizing the dielectric loss, resulting in a 246% increase in the electromechanical conversion efficiency. This, to a certain extent, breaks through the trade-off limitation between the dielectric constant and dielectric loss of traditional dielectric materials and provides a new strategy for the design of high-performance PTMs.

Further investigation was conducted on the impact of frequency and load on the output performance of the DCCNF4-based TENG. As shown in Figure S6, the V_{oc} and Q_{sc} remained relatively stable with variations in frequency and load, while the I_{sc} increased with the rise in frequency and load. This indicates that the DCCNF4-based TENG possesses the capability of wide-band mechanical energy harvesting and can optimize its output performance through working condition regulation. Benefiting from the thermally reversible nature of the dynamic covalent cross-linked network, the mechanically scratched surface of DCCNF4 could self-healing after 24 h of heat treatment at 100°C (Figure 2j). Triboelectric testing confirmed that there was almost no difference in output performance before and after repair (Figure 2j), demonstrating excellent functional recovery ability. Considering the stringent requirements for output stability in the practical applications of TENGs, the cyclic durability was evaluated under a working condition of 2 Hz@10 N. The results revealed that the DCCNF4-based TENG could operate continuously and stably for over 20 000 cycles (Figure 2k), exhibiting outstanding mechanical stability and durability.

16136829, 0, Downloaded from https://onlinelibrary.wiley.com/doi/10.1002/smll.75667 by Beihang University (Buaa), Wiley Online Library on [23/09/2026]. See the Terms and Conditions (https://onlinelibrary.wiley.com/terms-and-conditions) on Wiley Online Library for rules of use; OA articles are governed by the applicable Creative Commons License

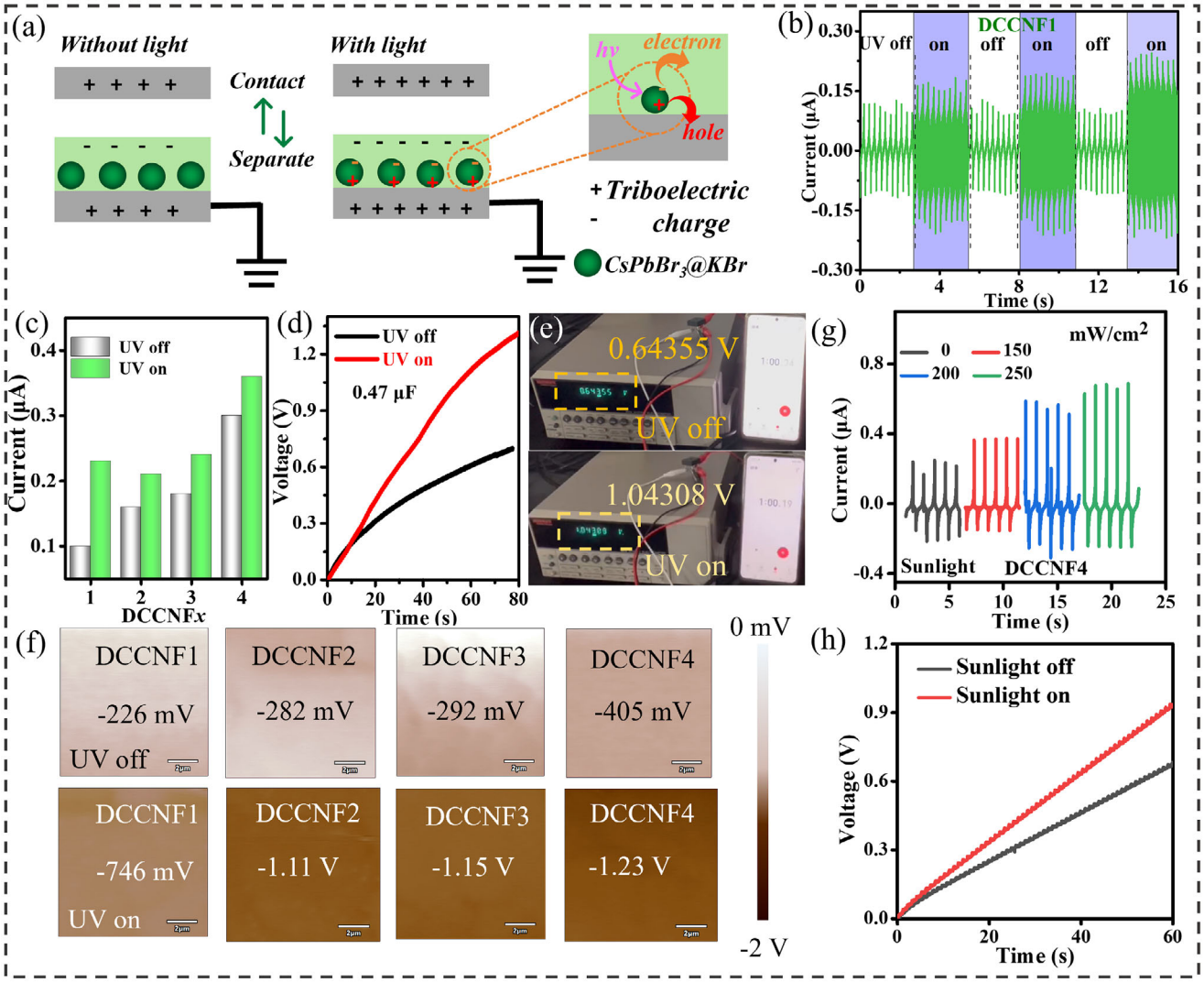


FIGURE 3 | (a) Working mechanism of $CsPbBr_3$@KBr doped DCCNF-based single-electrode TENGs under light irradiation. (b,c) I_{sc} of the series DCCNFs with and without UV light irradiation. (d,e) Charging curves of a 0.47 μF capacitor powered by the DCCNF4-based TENG with and without UV light irradiation. The optical photo on the right shows the voltage value reached by the capacitor after approximately 60 s of charging. (f) KPFM images of the series DCCNFs with and without UV light irradiation. (g) I_{sc} of the DCCNF4-based TENG under varying sunlight intensities. (h) Charging curves of a 1 μF capacitor powered by the DCCNF4-based TENG with and without sunlight irradiation (150 mW/cm^2).

2.4 | Photoinduced Enhanced Triboelectric Characteristics and Applications of DCCNF-Based TENGs

Halide perovskite materials, leveraging their excellent photoelectric and dielectric properties along with high carrier mobility, can significantly enhance the output current density. Crucially, perovskite-based TENGs exploit this multifunctionality to boost output performance via photoelectric-triboelectric coupling effects without complex device integration, demonstrating substantial potential for composite TENG applications [38, 39]. As illustrated in Figure 3a, under illumination, the $CsPbBr_3$@KBr doped DCCNF-based TENGs operate under a dual energy conversion mechanism—primary triboelectric conversion and secondary photoelectric conversion. Fundamentally distinct from dark conditions, photon absorption by $CsPbBr_3$@KBr generates photogenerated carriers, creating abundant electron-hole pairs. Driven by TENG's contact electrification-induced built-in electric field, photoelectrons migrate toward the triboelectric interface while holes remain localized within the DCCNF layer. That is, the built-in electric field accelerates the separation of photogenerated carriers, and photoelectrons synergistically enhance the interface charge density with triboelectric charges, thereby improving the device's output performance through the synergistic effect of photoelectric and triboelectric effects [24, 64]. As shown in Figure 3b,c and Figure S7, under UV light irradiation, $CsPbBr_3$@KBr-doped DCCNFs exhibit markedly increased output current density, confirming photoelectric-triboelectric coupling enhancement. Figure 3d,e demonstrate that UV-irradiated DCCNF4-based TENG charges a 0.47 μF capacitor to 1.04 V within 60 s—representing a 62.5% enhancement over dark conditions (0.64 V). KPFM characterization further validates this mechanism (Figure 3f and Figure S8): the pronounced negative shift in surface potential under illumination confirms charge

16136829, 0, Downloaded from https://onlinelibrary.wiley.com/doi/10.1002/smll.75667 by Beihang University (Buaa), Wiley Online Library on [23/09/2026]. See the Terms and Conditions (https://onlinelibrary.wiley.com/terms-and-conditions) on Wiley Online Library for rules of use; OA articles are governed by the applicable Creative Commons License

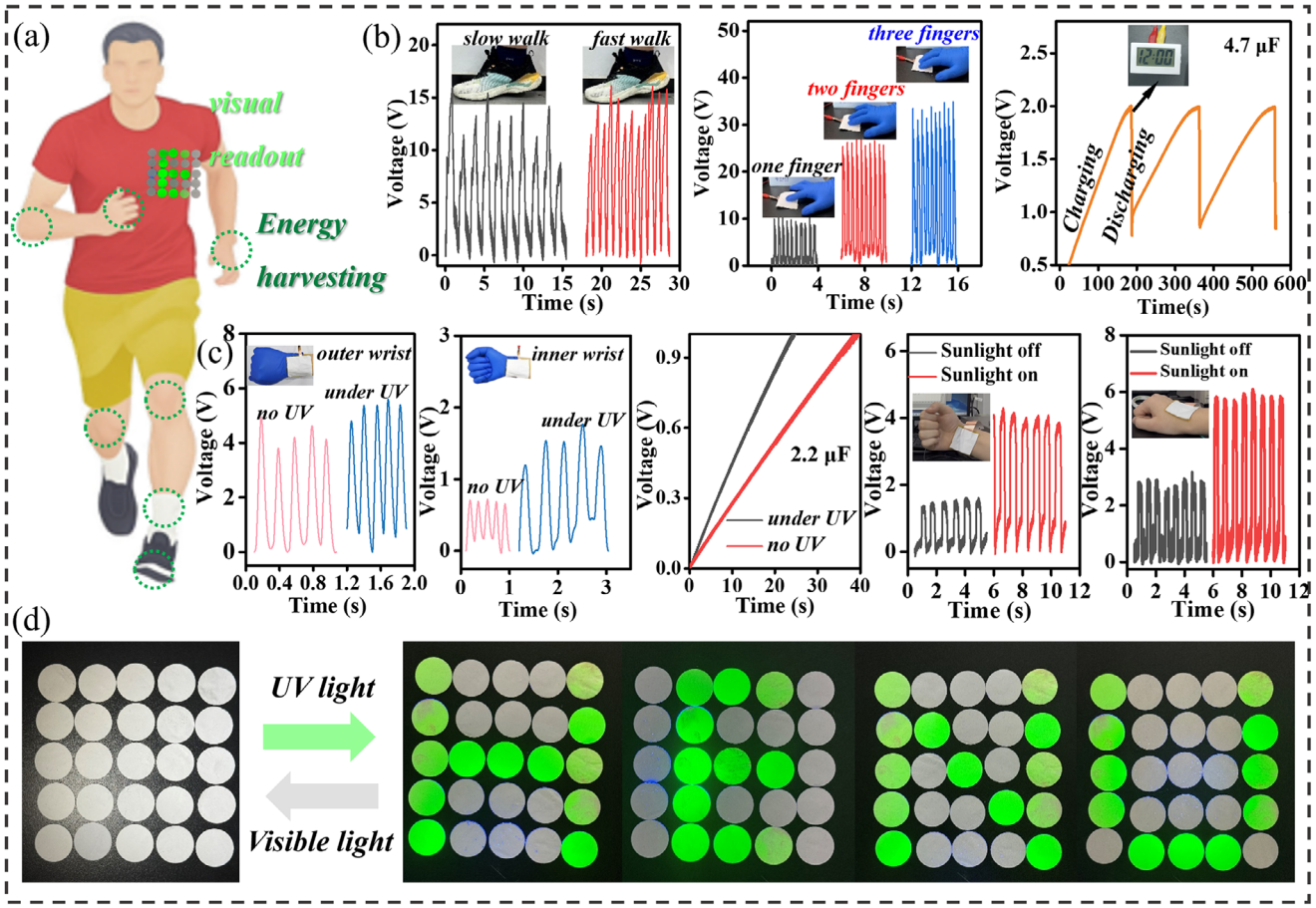


FIGURE 4 | The application of DCCNF-based photoinduced enhanced TENG devices. (a–c) Harvesting body movement energy and light energy, and supply power to commercial electronic devices. (d) Application of DCCNF-based wearable photoluminescent visual readout in dark conditions.

compensation through the built-in electric field-driven photogenerated carrier migration to the interface. More significantly, as shown in Figure 3g,h and Videos S1–S5, under varying simulated sunlight irradiation, the I_{sc} of the DCCNF$_4$ increases progressively with light intensity, reaching approximately 0.67 μA, a 201% enhancement relative to dark conditions. Meanwhile, the DCCNF4-based TENG charges a 1 μF capacitor to 0.94 V within 60 s under sunlight, a 40% improvement over the dark condition. These results underscore the practical viability of perovskite-based TENGs for outdoor self-powered systems, where abundant sunlight can be simultaneously harvested to boost electrical output. The comprehensive comparison in Table S1 clearly highlights the performance and functional advantages of our work over previously reported devices. This study provides a new paradigm for high-performance photoelectric-triboelectric coupled TENGs, with significant implications for hybrid energy harvesting and self-powered detection systems.

To evaluate the practical value of the multifunctional DCCNF-based TENG device prepared in this study for the synergistic collection of mechanical and photo energy, it was integrated onto different human body locations for biomechanical energy harvesting and dynamic motion sensing (Figure 4a). Distinct biomechanical signals generated by differential body part stimulations and movement patterns enable precise human motion detection [48]. As demonstrated in Figure 4b,c, the device can sense motions of different body parts, effectively harvest human motion energy, and repeatedly power a commercial electronic watch in a cyclic manner. Moreover, the output signals of the DCCNF-based TENG devices attached to different parts of the human body vary, and the output signals are significantly enhanced under different illumination (UV and sunlight). This indicates that, through the coupling of photoelectric and triboelectric effects, the DCCNF-based TENG device not only improves energy capture efficiency, facilitating the development of self-powered wearable devices, but also possesses the potential for dual-mode sensing of force and ambient light intensity.

Given that CsPbBr$_3$@KBr is colorless and exhibits no photoluminescence under daylight but emits bright green light under a 365 nm UV excitation, further exploration was carried out on the applications of the fabricated DCCNF-based TENG in intelligent display, information encryption, and visual readout. As illustrated in Figure 4d, a 5 × 5 dot matrix was constructed using DCCNF4 (diameter 1 cm) as the luminescent pixels and DCCNF0 (diameter 1 cm) as the blank pixels. By arranging the pixels in different combinations, various types of information encryption and transmission can be achieved. The dot matrix does not display any pattern information under daylight, meaning no information is transmitted, thus realizing pattern encryption. Under 365 nm UV excitation, the DCCNF4 luminescent pixels can clearly display the letters “H,” “E,” “N,” and “U,” achieving

16136829, 0, Downloaded from https://onlinelibrary.wiley.com/doi/10.1002/smll.75667 by Beihang University (Buaa), Wiley Online Library on [23/09/2026]. See the Terms and Conditions (https://onlinelibrary.wiley.com/terms-and-conditions) on Wiley Online Library for rules of use; OA articles are governed by the applicable Creative Commons License

intelligent display and visual readout [65, 66]. In conclusion, the DCCNF-based TENG device prepared in this study can efficiently and synchronously harvest human motion energy and photo energy to power wearable electronic devices, and simultaneously realize information encryption and visual readout, which holds broad application prospects in the field of intelligent, wearable, self-powered electronic devices.

3 | Conclusions

This study successfully fabricated a series of multifunctional and synergistically optimized textile-based TENGs (DCCNF-based TENGs). A dynamic covalent cross-linked polymer network was utilized as the triboelectric matrix, which ingeniously balanced the contradiction between the durability and recyclability of PTMs. $CsPbBr_3$@KBr all-inorganic photoluminescent perovskite was used as the functional filler. The KBr salt shell created a Br-rich environment to passivate surface defects and, together with the DA adduct, acted as a protective matrix to enhance the environmental stability of the perovskite material, achieving functional coupling and synergistic optimization of the triboelectric and photoelectric effects. The triboelectric output of the device reached its peak when the doping amount of $CsPbBr_3$@KBr was 4 wt.%. Compared with undoped DCCNF0, the V_{oc}, I_{sc}, and Q_{sc} of DCCNF4-based TENG increased by 2.25-fold, 5.78-fold, and 3.13-fold, respectively. Notably, under UV and sunlight irradiation, the synergistic effect of the photoelectric-triboelectric effects significantly improved the current density of the series DCCNFs, and these samples exhibited a unique photoluminescence phenomenon, further expanding the functional characteristics of the device. In summary, the DCCNF-based TENG devices possess excellent energy harvesting and conversion capabilities, which can efficiently and synchronously capture human motion energy and light energy and significantly enhance their output performance through the photo-induced effect, thereby providing a stable and efficient energy supply for wearable electronic devices. Moreover, it can create information encryption and visual reading functions, offering an innovative platform for the next generation of sustainable smart wearable systems, which shows broad application prospects in fields such as wearable electronics and intelligent sensing.

4 | Experimental Section

4.1 | Preparation of $CsPbBr_3$@KBr Doped Multifunctional Dynamic Covalently Crosslinked Nanofibers (DCCNFs)

The multifunctional DCCNFs doped with $CsPbBr_3$@KBr were fabricated via electrospinning technology, and the resulting nanofiber membranes were utilized as triboelectric functional layers. The detailed preparation procedure is outlined as follows: Initially, BMI was added to a 25 wt.% FMA-*co*-BMA/DMF solution at a 1:0.6 molar ratio relative to the furan groups in FMA-*co*-BMA. An appropriate amount of DMF was then supplemented to adjust the final solute mass fraction to 28 wt.%.

Subsequently, $CsPbBr_3$@KBr was incorporated into the solution at various mass fractions (0, 1, 2, 3, 4, and 5 wt.%), and the mixture was vigorously stirred to form a homogeneous $CsPbBr_3$@KBr/FMA-*co*-BMA/BMI composite solution. The resulting composite solution was then placed in a 60°C constant-temperature water bath to facilitate the DA reaction between FMA-*co*-BMA and BMI, with continuous heating for about 40 min. Following that, the above solution (with a room-temperature viscosity of approximately 80 cps) was used as the spinning solution for electrospinning $CsPbBr_3$@KBr-doped DCCNFs. After electrospinning, the nanofiber membranes were dried in a 60°C oven for 24 h to remove residual solvents and stabilize the nanofiber structure.

Therein, the mass fraction gradient of $CsPbBr_3$@KBr was set from 0 to 5 wt.%, with corresponding samples labeled as DCCNF0 to DCCNF5. The specific synthesis process of FMA-*co*-BMA and $CsPbBr_3$@KBr is detailed in the Supporting Information. The electrospinning process parameters were as follows: a feed rate of 1 mL/h, a voltage range of 15–18 kV, a collection distance of 20 cm, a collection duration of 1 h, with relative humidity and temperature controlled at ≤40% and 30 ± 5°C, respectively.

4.2 | Characterizations and Measurement

The relevant details are listed in Supporting Information.

Acknowledgements

This work was supported by the National Natural Science Foundation of China (No., 52125205, 52532005, 52250398 and W2641027), Postdoctoral Fellowship Program of CPSF (No. GZC20230681), Fund of Key Laboratory of Advanced Materials of Ministry of Education (No. Advmat-2411), National Key Research and Development (R&D) Program from Ministry of Science and Technology of China (No. 2024YFB3814100) and the Fundamental Research Funds for the Central Universities.

Conflicts of Interest

The authors declare no conflicts of interest.

Data Availability Statement

The data that support the findings of this study are available from the corresponding author upon reasonable request.

References

1. Y. Liu, J. Tao, Y. Mo, R. Bao, and C. Pan, "Ultrasensitive Touch Sensor for Simultaneous Tactile and Slip Sensing," *Advanced Materials* 36 (2024): 2313857, https://doi.org/10.1002/adma.202313857.

2. Q. Li, L. Zhang, C. Zhang, et al., "Compact, Robust, and Regulated-Output Hybrid Generators for Magnetic Energy Harvesting and Self-Powered Sensing Applications in Power Transmission Lines," *Energy & Environmental Science* 17 (2024): 2787–2799, https://doi.org/10.1039/D3EE04563C.

3. X. Huang, Y. Wang, and X. Zhang, "Ultrarobust, Hierarchically Anisotropic Structured Piezoelectric Nanogenerators for Self-Powered Sensing," *Nano Energy* 99 (2022): 107379, https://doi.org/10.1016/j.nanoen.2022.107379.

4. C. Wang, H. Guo, P. Wang, J. Li, Y. Sun, and D. Zhang, "An Advanced Strategy to Enhance TENG Output: Reducing Triboelectric Charge Decay," *Advanced Materials* 35 (2023): 2209895, https://doi.org/10.1002/adma.202209895.

16136829, 0, Downloaded from https://onlinelibrary.wiley.com/doi/10.1002/smll.75667 by Beihang University (Buaa), Wiley Online Library on [23/09/2026]. See the Terms and Conditions (https://onlinelibrary.wiley.com/terms-and-conditions) on Wiley Online Library for rules of use; OA articles are governed by the applicable Creative Commons License

5. G. Wu, X. Li, R. Bao, and C. Pan, "Innovations in Tactile Sensing: Microstructural Designs for Superior Flexible Sensor Performance," *Advanced Functional Materials* 34 (2024): 2405722, https://doi.org/10.1002/adfm.202405722.

6. W. Han, R. Nie, B. Yin, et al., "All Irradiance-Applicable, Perovskite Solar Cells-Powered Flexible Self-Sustaining Sensor Nodes for Wireless Internet-of-Things," *Advanced Functional Materials* 35 (2025): 2425697, https://doi.org/10.1002/adfm.202425697.

7. S. Shen, H. Wu, Z. Xu, et al., "Wearable Multifunctional Bilayer Nanofiber Films for Human Motion Energy Harvesting and Photothermal Therapy," *Advanced Functional Materials* 35 (2025): 2419645, https://doi.org/10.1002/adfm.202419645.

8. Y. Hao, C. Zhang, W. Su, et al., "Sustainable Materials Systems for Triboelectric Nanogenerator," *SusMat* 4 (2024): 244, https://doi.org/10.1002/sus2.244.

9. R. Cao, Y. Liu, H. Li, et al., "Advances in High-Temperature Operatable Triboelectric Nanogenerator," *SusMat* 4 (2024): 196.

10. Y. Zheng, T. Liu, J. Wu, et al., "Energy Conversion Analysis of Multilayered Triboelectric Nanogenerators for Synergistic Rain and Solar Energy Harvesting," *Advanced Materials* 34 (2022): 2202238, https://doi.org/10.1002/adma.202202238.

11. L. Liu, Y. Shang, A. Berbille, et al., "Self-Powered Sensing Platform Based on Triboelectric Nanogenerators towards Intelligent Mining Industry," *Nature Communications* 16 (2025): 5141, https://doi.org/10.1038/s41467-025-60418-9.

12. Y. Gao, L. He, D. Liu, et al., "Spontaneously Established Reverse Electric Field to Enhance the Performance of Triboelectric Nanogenerators via Improving Coulombic Efficiency," *Nature Communications* 15 (2024): 4167, https://doi.org/10.1038/s41467-024-48456-1.

13. Q. Guo, X. Yang, Y. Wang, W. Xu, J. Duan, and Q. Tang, "Dielectric Hole Collector Toward Boosting Charge Transfer of $CsPbBr_3$ Hybrid Nanogenerator by Coupling Triboelectric and Photovoltaic Effects," *Advanced Functional Materials* 31 (2021): 2101348, https://doi.org/10.1002/adfm.202101348.

14. Y. Zhao, S. Shen, R. Cao, et al., "Flexible Stretchable Tribo-Negative Films With Exceptional Output Performance for High-Temperature Energy Harvesting and Self-Powered Sensor," *Nano Energy* 114 (2023): 108654, https://doi.org/10.1016/j.nanoen.2023.108654.

15. X. Huang, B. Zhou, G. Sun, X. Yang, Y. Wang, and X. Zhang, "Upcycling of Plastic Wastes and Biomass to Mechanically Robust yet Recyclable Energy-Harvesting Materials," *Nano Energy* 116 (2023): 108843.

16. S. Shen, Y. Zhao, R. Cao, et al., "Triboelectric Polymer With Excellent Enhanced Electrical Output Performance over a Wide Temperature Range," *Nano Energy* 110 (2023): 108347, https://doi.org/10.1016/j.nanoen.2023.108347.

17. Y. Li, S. Xiao, Y. Luo, et al., "Advances in Electrospun Nanofibers for Triboelectric Nanogenerators," *Nano Energy* 104 (2022): 107884, https://doi.org/10.1016/j.nanoen.2022.107884.

18. K. Zhou, Y. Zhao, X. Sun, et al., "Ultra-Stretchable Triboelectric Nanogenerator as High-Sensitive and Self-Powered Electronic Skins for Energy Harvesting and Tactile Sensing," *Nano Energy* 70 (2020): 104546, https://doi.org/10.1016/j.nanoen.2020.104546.

19. K. R. S. Dinuwan Gunawardhana, R. B. V. B. Simorangkir, G. B. McGuinness, et al., "The Potential of Electrospinning to Enable the Realization of Energy-Autonomous Wearable Sensing Systems," *ACS Nano* 18 (2024): 2649–2684, https://doi.org/10.1021/acsnano.3c09077.

20. S. Wang, S. Ma, Q. Li, et al., "Facile In Situ Preparation of High-Performance Epoxy Vitrimer From Renewable Resources and Its Application in Nondestructive Recyclable Carbon Fiber Composite," *Green Chemistry* 21 (2019): 1484–1497, https://doi.org/10.1039/C8GC03477J.

21. H. Chen, Y. Hu, C. Luo, et al., "Spiroborate-Linked Ionic Covalent Adaptable Networks With Rapid Reprocessability and Closed-Loop Recyclability," *Journal of the American Chemical Society* 145 (2023): 9112–9117, https://doi.org/10.1021/jacs.3c00774.

22. S. Wang, N. Wang, and D. Kai, "In-Situ Forming Dynamic Covalently Crosslinked Nanofibers With One-Pot Closed-Loop Recyclability," *Nature Communications* 14 (2023): 1182, https://doi.org/10.1038/s41467-023-36709-4.

23. M. L. Lepage, C. Simhadri, C. Liu, et al., "A Broadly Applicable Cross-Linker for Aliphatic Polymers Containing C–H Bonds," *Science* 366 (2019): 875–878, https://doi.org/10.1126/science.aay6230.

24. Y. Yang, B. Xu, X. Yin, X. Liu, D. Tan, and Q. Wang, "Flexible Hybrid Nanogenerator Coupling of Triboelectric and Photovoltaic Effects Based on Fluoride Dielectric Regulation for Energy Harvesting," *Nano Energy* 126 (2024): 109707, https://doi.org/10.1016/j.nanoen.2024.109707.

25. H. Chen, L. J. Wayment, H. Jiang, et al., "Closed-Loop Recyclable Lithium and Sodium Conducting Covalent Adaptable Networks," *Angewandte Chemie International Edition* 64 (2025): 202425497, https://doi.org/10.1002/anie.202425497.

26. N. Jarach, M. Cohen, R. Gitt, H. Dodiuk, S. Kenig, and S. Magdassi, "Untying the Knot: A Fully Recyclable, Solvent-Free, Wide-Spectral Photocurable Thermoset Adhesive," *Advanced Materials* 37 (2025): 2502040, https://doi.org/10.1002/adma.202502040.

27. B. Li, C. Qu, S. Wang, et al., "Closed-Loop Recyclable Dynamic Covalent Crosslinked Nanofibrous Membranes for Efficient Oil/Water Separation," *Journal of Membrane Science* 693 (2024): 122378, https://doi.org/10.1016/j.memsci.2023.122378.

28. Z. Lei, H. Chen, S. Huang, L. J. Wayment, Q. Xu, and W. Zhang, "New Advances in Covalent Network Polymers via Dynamic Covalent Chemistry," *Chemical Reviews* 124 (2024): 7829–7906, https://doi.org/10.1021/acs.chemrev.3c00926.

29. S. Gu, Y.-F. Xiao, S.-H. Tan, et al., "Neighboring Molecular Engineering in Diels–Alder Chemistry Enabling Easily Recyclable Carbon Fiber Reinforced Composites," *Angewandte Chemie International Edition* 62 (2023): 202312638, https://doi.org/10.1002/anie.202312638.

30. F. Jiang, G. Thangavel, J. P. Lee, et al., "Self-Healable and Stretchable Perovskite-Elastomer Gas-Solid Triboelectric Nanogenerator for Gesture Recognition and Gripper Sensing," *Science Advances* 10 (2024): adq5778, https://doi.org/10.1126/sciadv.adq5778.

31. S. Iabal, M. M. Rehman, Z. Abbas, et al., "High Performance Triboelectric Nanogenerator Based on Metal-Organic Framework Composites for IoT-Assisted Wireless Healthcare Monitoring," *Energy & Environmental Materials* 8 (2025): 70010.

32. Z. Wang, D. Wu, M. Chi, et al., "Thermally Robust Aramid Triboelectric Materials Enabled by Heat-Induced Cross-Linking," *Advanced Functional Materials* 35 (2025): 2413719, https://doi.org/10.1002/adfm.202413719.

33. F. Jiang and P. S. Lee, "Performance Optimization Strategies of Halide Perovskite-Based Mechanical Energy Harvesters," *Nanoscale Horizons* 7 (2022): 1029–1046, https://doi.org/10.1039/D2NH00229A.

34. C. Ma, B. Kim, S.-W. Kim, and N.-G. Park, "Dynamic Halide Perovskite Heterojunction Generates Direct Current," *Energy & Environmental Science* 14 (2021): 374–381, https://doi.org/10.1039/D0EE03487H.

35. Z. Wei, L. Ding, N. Sun, et al., "Lead-Free $CsBi_3I_{10}$ Perovskite Based Photo-Enhanced Triboelectric Nanogenerator," *Nano Energy* 108 (2023): 108209, https://doi.org/10.1016/j.nanoen.2023.108209.

36. M. Kim, S. Lee, V. A. Cao, M. C. Kim, and J. Nah, "Performance Enhancement of Triboelectric Nanogenerators via Photo-Generated Carriers Using a Polymer-Perovskite Composite," *Nano Energy* 112 (2023): 108474, https://doi.org/10.1016/j.nanoen.2023.108474.

16136829, 0, Downloaded from https://onlinelibrary.wiley.com/doi/10.1002/smll.75667 by Beihang University (Buaa), Wiley Online Library on [23/09/2026]. See the Terms and Conditions (https://onlinelibrary.wiley.com/terms-and-conditions) on Wiley Online Library for rules of use; OA articles are governed by the applicable Creative Commons License

37. Y. Wang, X. Yang, X. Yu, et al., "Triboelectric Charging Behaviors and Photoinduced Enhancement of Alkaline Earth Ions Doped Inorganic Perovskite Triboelectric Nanogenerators," *Nano Energy* 77 (2020): 105280, https://doi.org/10.1016/j.nanoen.2020.105280.

38. J. Yuan, X. Yang, D. Zheng, et al., "Perovskite Quantum Dot-Based Tandem Triboelectric-Solar Cell for Boosting the Efficiency and Rain Energy Harvesting," *Nano Energy* 110 (2023): 108341, https://doi.org/10.1016/j.nanoen.2023.108341.

39. L. Ding, Z. Wei, X. Zeng, K. Fang, and G. Wang, "Lead-Free Perovskite $Cs_3Sb_2Cl_3I_6$ via Additive Engineering for Enhancing Output Performance of Optoelectronic and Triboelectric Coupled Nanogenerator," *Nano Energy* 133 (2025): 110451, https://doi.org/10.1016/j.nanoen.2024.110451.

40. H. Yuan, Z. Xiao, J. Wan, et al., "A Rolling-Mode Al/$CsPbBr_3$ Schottky Junction Direct-Current Triboelectric Nanogenerator for Harvesting Mechanical and Solar Energy," *Advanced Energy Materials* 12 (2022): 2200550, https://doi.org/10.1002/aenm.202200550.

41. W. Zhao, Q. Liu, Z. Tian, et al., "Boosting Tribo-Photovoltaic Effect in Perovskite Triboelectric Nanogenerators by Regulating Built-in Potential Through p-n Junctions," *Nano Energy* 136 (2025): 110723, https://doi.org/10.1016/j.nanoen.2025.110723.

42. S. Huang, L. Shi, T. Zou, et al., "Controlling Performance of Organic–Inorganic Hybrid Perovskite Triboelectric Nanogenerators via Chemical Composition Modulation and Electric Field-Induced Ion Migration," *Advanced Energy Materials* 10 (2020): 2002470, https://doi.org/10.1002/aenm.202002470.

43. W. Fu, A. G. Ricciardulli, Q. A. Akkerman, et al., "Stability of Perovskite Materials and Devices," *Materials Today* 58 (2022): 275–296, https://doi.org/10.1016/j.mattod.2022.06.020.

44. E. Akman, T. Ozturk, W. Xiang, et al., "The Effect of B-Site Doping in All-Inorganic $CsPbI_xBr_{3-x}$ Absorbers on the Performance and Stability of Perovskite Photovoltaics," *Energy & Environmental Science* 16 (2023): 372–403, https://doi.org/10.1039/D2EE01070D.

45. H. Wang, Y. Yu, X. Yang, et al., "A Smart Mechanical-Energy Harvesting and Self-Heating Textile Device for Photo-Thermal Energy Utilization," *EcoMat* 5 (2023): 12337, https://doi.org/10.1002/eom2.12337.

46. V. G. Muir and J. A. Burdick, "Chemically Modified Biopolymers for the Formation of Biomedical Hydrogels," *Chemical Reviews* 121 (2021): 10908–10949, https://doi.org/10.1021/acs.chemrev.0c00923.

47. C. R. Ratwani, A. R. Kamali, and M. A. Abdelkader, "Self-Healing by Diels-Alder Cycloaddition in Advanced Functional Polymers: A Review," *Progress in Materials Science* 131 (2023): 101001, https://doi.org/10.1016/j.pmatsci.2022.101001.

48. L. Chen, M. He, W. Gong, et al., "Robust Salt-Shelled Metal Halide for Highly Efficient Photoluminescence and Wearable Real-Time Human Motion Perception," *Nano Energy* 108 (2023): 108235, https://doi.org/10.1016/j.nanoen.2023.108235.

49. Z. Xu, W. Peng, J. Huang, J. Shen, J. Guo, and A. Hu, "Photoinduced Formal [4 + 2] Cycloaddition of Two Electron-Deficient Olefins and its Application to the Synthesis Of Lucidumone," *Nature Communications* 15 (2024): 9748, https://doi.org/10.1038/s41467-024-54117-0.

50. Q. He, Z. Xu, H. Fang, et al., "Catalytic Ring Expansion of Furyl Hydrosilanes: Synthesis of 1,2-Oxasilines as Diels-Alder Diene Components," *Angewandte Chemie International Edition* 64 (2025): 202425232, https://doi.org/10.1002/anie.202425232.

51. P. Ge, L. Zhang, W. Zhao, Y. Yang, W. Sun, and X. Ji, "Interfacial Bonding of Metal-Sulfides With Double Carbon for Improving Reversibility of Advanced Alkali-Ion Batteries," *Advanced Functional Materials* 30 (2020): 1910599, https://doi.org/10.1002/adfm.201910599.

52. Y. Byun and A. Coskun, "Epoxy-Functionalized Porous Organic Polymers via the Diels–Alder Cycloaddition Reaction for Atmospheric Water Capture," *Angewandte Chemie International Edition* 57 (2018): 3173–3177, https://doi.org/10.1002/anie.201800380.

53. L. Yang, P. Cai, X. Jin, Z. Wang, H. Zhou, and N. Huang, "Phenolic Resin-Type Microporous Organic Polymers for High-Performance Carbon Dioxide Adsorption," *Chemistry—An Asian Journal* 20 (2025): 202401288, https://doi.org/10.1002/asia.202401288.

54. J. Li, W. Yang, P. Xu, D. Niu, and P. Ma, "Recyclable High-Performance Thermosetting Plastics From Isosorbide Based on Diels–Alder Reaction," *Industrial & Engineering Chemistry Research* 64 (2025): 7002–7012, https://doi.org/10.1021/acs.iecr.4c04639.

55. Y. Nie, M. Li, S. Li, et al., "Design, Fabrication and Characterization of Dynamic Covalent Polymer Networks Containing Reversible Diels-Alder Adducts Derived From Vegetable Oil and Furfural," *Polymer Testing* 127 (2023): 108196, https://doi.org/10.1016/j.polymertesting.2023.108196.

56. Y. Lin, Z. Lin, S. Lv, et al., "A Nd@C82–Polymer Interface for Efficient and Stable Perovskite Solar Cells," *Nature* 642 (2025): 78–84, https://doi.org/10.1038/s41586-025-08961-9.

57. Z. Zhang, C. Hu, Y. Li, et al., "F for Fantastic: Fostering Stability and Efficiency in Perovskite Solar Cells via Comb-Like Perfluoroalkyl- g -Polyethylenimine Additive," *Small Methods* 9 (2025): 2400643, https://doi.org/10.1002/smtd.202400643.

58. R. Sun, S. Chen, Q. He, et al., "A Stepwise Melting-Polymerizing Molecule for Hydrophobic Grain-Scale Encapsulated Perovskite Solar Cell," *Advanced Materials* 37 (2025): 2410395, https://doi.org/10.1002/adma.202410395.

59. X. Sun, L. Dong, J. Liu, T. Hou, and S. Chen, "Multi-Scale Modified PVDF/Ag@C Layer Based on Dielectric Doping and Plasma Treatment for High-Performance Triboelectric Nanogenerators and Self-Powered Water Sterilization," *Nano Energy* 124 (2024): 109511, https://doi.org/10.1016/j.nanoen.2024.109511.

60. J. Wang, S. Xu, G. Li, et al., "Effectively Inhibiting Charge Injection and Dielectric Loss of High Permittivity Inorganic Materials by Rationally Coating Organic Polymer for Achieving High Output Charge Density," *Advanced Energy Materials* 14 (2024): 2400429, https://doi.org/10.1002/aenm.202400429.

61. Z. Peng, X. Xiao, J. Song, et al., "Improving Relative Permittivity and Suppressing Dielectric Loss of Triboelectric Layers for High-Performance Wearable Electricity Generation," *ACS Nano* 16 (2022): 20251–20262, https://doi.org/10.1021/acsnano.2c05820.

62. W. Cho, S. Kim, H. Lee, et al., "High-Performance Yet Sustainable Triboelectric Nanogenerator Based on Sulfur-Rich Polymer Composite With MXene Segregated Structure," *Advanced Materials* 36 (2024): 2404163, https://doi.org/10.1002/adma.202404163.

63. H. Wu, Z. Xu, R. Cao, et al., "Multipurpose Smart Textile With Integration of Efficient Energy Harvesting, All-Season Switchable Thermal Management and Self-Powered Sensing," *Advanced Functional Materials* 35 (2025): 09281, https://doi.org/10.1002/adfm.202509281.

64. W. Lu, X. Pan, W. L. Ong, K. Zeng, and G. W. Ho, "Enhanced Triboelectricity through Visible-Light-Induced Surface Charges in BTO-Polymer Hybrid for Coexistence Solar-Mechanical Energy Harvesting," *Nano Energy* 128 (2024): 109867, https://doi.org/10.1016/j.nanoen.2024.109867.

65. Y. Zhao, X. Yang, L. Yang, et al., "Advanced Optical Information Encryption Enabled by Polychromatic and Stimuli-Responsive Luminescence of Sb-Doped Double Perovskites," *Advanced Science* 11 (2024): 2308390, https://doi.org/10.1002/advs.202308390.

66. L. Cheng, Y. Yun, J. Chi, et al., "Patterning-Induced Encapsulation of Stable Perovskite Quantum Dots With Controllable Morphology for Infor-

16136829, 0, Downloaded from https://onlinelibrary.wiley.com/doi/10.1002/smll.75667 by Beihang University (Buaa), Wiley Online Library on [23/09/2026]. See the Terms and Conditions (https://onlinelibrary.wiley.com/terms-and-conditions) on Wiley Online Library for rules of use; OA articles are governed by the applicable Creative Commons License

mation Encryption," *Advanced Functional Materials* 35 (2025): 2500189, https://doi.org/10.1002/adfm.202500189.

Supporting Information

Additional supporting information can be found online in the Supporting Information section.

Supporting File 1: smll75667-sup-0001-SuppMat.docx.
Supporting File 2: smll75667-sup-0002-VideoS1.mp4.
Supporting File 3: smll75667-sup-0003-VideoS2.mp4.
Supporting File 4: smll75667-sup-0004-VideoS3.mp4.
Supporting File 5: smll75667-sup-0005-VideoS4.mp4.
Supporting File 6: smll75667-sup-0006-VideoS5.mp4.

16136829, 0, Downloaded from https://onlinelibrary.wiley.com/doi/10.1002/smll.75667 by Beihang University (Buaa), Wiley Online Library on [23/09/2026]. See the Terms and Conditions (https://onlinelibrary.wiley.com/terms-and-conditions) on Wiley Online Library for rules of use; OA articles are governed by the applicable Creative Commons License